Evaluation of Approaches to Solving Electrocardiographic Imaging Problem

M Milanic[1], V Jazbinsek[2], DF Wang[3], J Sinstra[3], RS MacLeod[3,4], DH Brooks[5], R Hren[2,6]

[1]Jozef Stefan Institute, Ljubljana, Slovenia
[2]Institute of Mathematics, Physics, and Mechanics, University of Ljubljana, Ljubljana, Slovenia
[3]Scientific Computing and Imaging Institute, University of Utah, Salt Lake City, UT, USA
[4]Nora Eccles Harrison Cardiovascular Research and Training Institute, University of Utah, Salt Lake City, UT, USA
[5]Dept of Electrical and Computer Engineering, Northeastern University, Boston, MA, USA
[6]Dept of Physics, University of Ljubljana, Ljubljana, Slovenia

Abstract

Electrocardiographic imaging (ECGI) is a widely used method of computing potentials on the epicardium from measured or simulated potentials on the torso surface. The main challenge of the electrocardiographic imaging problem lies in its intrinsic ill-posedness, and many regularization techniques have been developed to smooth out the solution. It is still an ongoing research subject to choose proper regularization methods and to determine their proper amount for obtaining clinically acceptable solutions. This study systematically compares various regularization techniques for the ECGI problem under a unified simulation framework. The framework consists of an electrolytic human torso tank containing a live canine heart, with the cardiac source being modeled by potentials measured on a cylindrical cage placed around the heart. We tested 14 different regularization techniques to solve the inverse problem of recovering epicardial potentials, and found that non-quadratic methods (total variation algorithms) were the most robust and resulted in the lowest reconstruction errors.

1. Introduction

In clinical practice, physicians deduce from a limited number of electrocardiographic signals complex electrical activities of the heart, which are usually simplified in the form of single-dipole, multi-dipole or potential distribution models. Such approach to solving the electrocardiographic inverse problem, despite often qualitative, still represents the cornerstone of a day-to-day diagnosis.

During the past 30 years, many research efforts have been devoted to exploring and validating the utility of electrocardiographic imaging, where potential distribution on the epicardial surface is inversely computed from a large number of electrocardiograms measured both on the anterior and posterior torso surface. Epicardial potentials have been recognized to directly reflect the underlying cardiac activity and could provide an effective means for localizing regional cardiac events. Electrocardiographic imaging problem, however, is inherently ill-posed in a sense that small errors in body-surface measurements may result in unbounded errors in the reconstruction of epicardial potentials. Given that the electrocardiography community has developed a plethora of regularization techniques to tackle the ill-posedness and to gauge the rapidly oscillating inverse solutions [1-5], there is a growing need to compare, structure and unify those diversified regularization methods by using the same volume conductor and the same cardiac source models.

This paper systematically evaluates the performance of 14 different regularization techniques using a realistic human torso model. We compared boundary element method and finite element method, two predominant methodologies in computing the geometrical and electrical properties of the torso volume conductor.

2. Methods

The electric potential field induced by cardiac activities can be modeled by a generalized Laplace's equation defined over the torso-shaped volume conductor subject to Cauchy boundary conditions [1-4]. Assuming the human torso is homogeneous and isotropic, this boundary value problem is solved by the boundary element method (BEM), which relates the potentials at

the torso nodes (expressed as an m-dimensional vector Φ_B) to the potentials at the epicardial nodes (expressed as an n-dimensional vector Φ_E),

$$\Phi_B = \mathbf{A}\,\Phi_E \ , \qquad (1)$$

where **A** is the transfer coefficient matrix (m * n) and n < m. The transfer coefficient matrix depends entirely on the geometric integrands, which can be calculated analytically. The finite element method (FEM) results in similar formalism as in (1) with the difference that the FEM discretizes the volume between the torso and epicardial surfaces into tetrahedral elements and can thereby take into account the electrical anisotropies of the volume conductor.

The matrix **A** is ill-conditioned, i.e., its singular values are limiting to zero with no particular gap of separation in the singular value spectrum, yielding a highly unstable solution. Regularization is needed to tackle the ill-posedness and control the wild oscillations in the inverse solution. We analyzed in a unified computational framework 14 regularization methods, which are summarized in Table 1. For the sake of structuring, we organized these regularization techniques in 3 groups: Tikhonov-based regularizations, iterative methods, and non-quadratic regularizations.

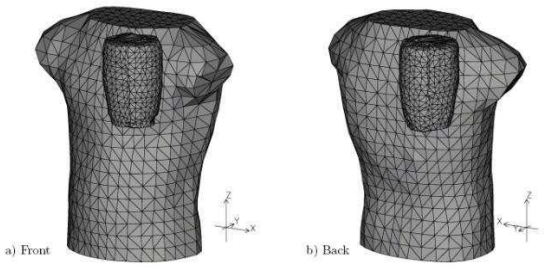

Figure 1. Geometries of the torso and cylindrical cage surfaces. Data recorded at 602 leads of the cylindrical cage were used to compute torso potentials at 771 nodes using BEM and FEM.

Our experimental protocol consisted of the following steps:

Step 1. We modeled the cardiac source by using a live canine heart which was retrogradely perfused via the aorta of another supportive dog. The heart was then suspended in the correct anatomical position in an electrolytic tank shaped like an adolescent thorax. We recorded electric potentials (at 1 kHz) from a 602-lead cylindrical cage enveloping the suspended canine heart and regarded the cage as the "epicardial" surface. Fig. 1 shows the geometries of torso and cylindrical cage. Data were collected during a sinus rhythm, with the sample epochs of 4-7 seconds in duration.

Step 2. We obtained Eq.(1) by means of the BEM and FEM respectively. We then calculated the torso potentials at 771 nodes from the cylindrical cage potentials. Both methods assumed the volume conductor was homogeneous and isotropic. Three measurement noise levels (20 dB, 40 dB, 60 dB) were added to the torso potentials to mimic experimental measurement conditions.

Table 1. Summary of 14 regularization techniques employed in our study. Techniques are subdivided into 3 main categories: Tikhonov-based regularizations (Group A), iterative methods (Group B), and non-quadratic methods (Group C).

Group	Acronym	Short description	Ref.
	ZOT	Zero-order Tikhonov	[6,7]
A	FOT	First-order Tikhonov	[4]
	SOT	Second-order Tikhonov	[7]
	ZCG	Zero-order Conjugate Gradient	[8]
	FCG	First-order Conjugate Gradient	[8]
	SCG	Second-order Conjugate Gradient	[8]
B	ZLSQR	Zero-order LSQR	[9]
	FLSQR	First-order LSQR	[9]
	SLSQR	Second-order LSQR	[9]
	TSVD	Truncated Singular Value Decomposition	[10]
	ν	ν-method	[10]
	FTV	Total Variation	[2,4]
C	STV	Total Variation with Laplacian	[2,4]
	LASSO	Least Absolute Selection and Shrinkage Operator	[11]

Step 3. The 602-lead cylindrical cage potentials were reconstructed by the 14 regularization techniques summarized in Table 1. We used the transfer matrix resulting from the BEM and the FEM, respectively.

Step 4. We evaluated the accuracy of the inverse solution in terms of its normalized rms (root-mean-square) error RE = $\|\Phi_E^c - \Phi_E^m\|_2 / \|\Phi_E^m\|_2$, and the correlation coefficient, CC = $\Phi_E^c \cdot \Phi_E^m / \|\Phi_E^c\|_2 \|\Phi_E^m\|_2$, where Φ_E^m is the measured cylindrical-cage potentials Φ_E^c is the computed potentials. We also examined the qualitative features of potential maps, both measured and inversely computed ones (e.g., areas of negative potentials, positions of extrema).

3. Results

Table 2 illustrates reconstruction results during the initial phase of the QRS complex, from the Q-onset to the peak of the Q-wave, using the BEM with 40-dB input noise. Despite the low-signal-to-noise ratio after the onset, the normalized RMS error of the reconstructed cage potentials ranged 0.22-0.36, and the correlation coefficients ranged 0.93-0.98, depending on the regularization technique used. It is evident that the most robust performance throughout the sequence was attained by the non-quadratic methods, either in the form of the total variation method (FTV) or the total variation algorithm, whose gradient operator was replaced by a Laplacian operator (STV).

Figure 2 depicts the body-surface potentials, the measured and calculated cage potentials at 5 ms after the onset of the Q wave. The simulation was carried out by the BEM, and the cage potentials were inversely computed by the FTV and STV. The body-surface potentials exhibited initial anterior maximum, resulting from the septal activation of the left ventricle. Both FTV and STV captured well the qualitative features of the cage potentials, with STV providing smoother solutions.

Table 3 summarizes results for standard reference points of the sinus rhythm (peaks of P, R, S, and T waves), again using the BEM with 40-dB input noise. Similar to Table 2, both non-quadratic regularization techniques (FTV, STV) performed consistently better than other 12 methodologies tested. There were, however, time instants when there were little differences among various regularization techniques, and when some Tikhonov regularizations (FOT, SOT) and iterative regularizations (FCG, SCG, FLSQR, SLSQR) were on a par with the non-quadratic techniques. Closer inspection of the cage potentials revealed that during those time instants, potential distributions were dipolar (i.e., exhibiting only a single maximum and minimum) and had rather simple spatial features (e.g., well separated extrema). Even in such cases, results suggest that FTV and STV still outperformed other techniques when the noise level was increased from 40 dB to 20 dB.

Comparison between BEM and FEM showed little difference, with BEM performing somewhat better than FEM. The difference between both methods was due to lower condition number of matrix **A** generated by the BEM than that by the FEM (by a factor of 73.1). Note that our comparison was based on an isotropic and homogeneous volume conductor model. The FEM is superior to the BEM in incorporating complex electric properties of the volume conductor.

Computational times of individual regularization techniques varied, with the iterative methods being the fastest (2 sec per reconstruction on average). Since Tikhonov and non-quadratic regularizations employ penalty functions, we needed to compute a large number (typically 20 to 40) of regularized solutions before determining the optimal one. Consequently, it took on average 8 sec per reconstruction when using Tikhonov and 180 sec when using FTV and STV. Among non-quadratic methods, LASSO required the least computational time (less than 2 sec per reconstruction).

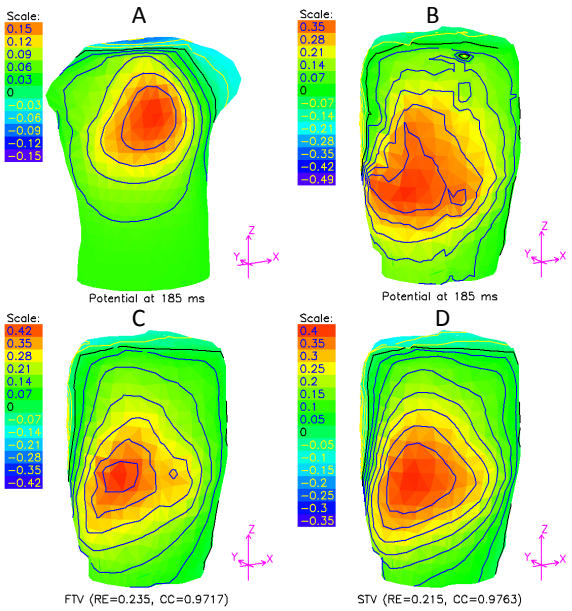

Figure 2. Potential distributions at 5 ms after the onset of the Q wave. (A) Torso potentials computed from the measured cylindrical cage potentials using boundary element method (BEM). (B) Measured cylindrical cage potentials. (C) Inversely computed cylindrical cage potentials using the totals variation method (FTV). (D) Inversely computed cylindrical cage potentials using the totals variation algorithm with the Laplacian instead of a gradient operator (STV).

Table 2. Root-mean-square (rms) errors for reconstruction results during the initial phase of the QRS complex, from the Q-onset to the peak of the Q-wave, in the presence of a 40-dB noise and when using BEM. Q_5 refers to the potential distributions at 5 ms after the Q-onset; the same applies to Q_{10} and Q_{15}; Q_{pk} refers to the distributions at the peak of the Q-wave. See Table 1 for explanations of acronyms describing regularization methods.

	ZOT	FOT	SOT	ZCG	FCG	SCG	ZLSQR	FLSQR	SLSQR	TSVD	ν	FTV	STV	LASSO
Q_5	0.32	0.22	0.22	0.32	0.25	0.25	0.32	0.25	0.25	0.33	0.32	0.23	0.22	0.36
Q_{10}	0.26	0.11	0.10	0.26	0.11	0.11	0.26	0.11	0.11	0.27	0.26	0.15	0.12	0.26
Q_{15}	0.30	0.18	0.16	0.26	0.19	0.15	0.26	0.19	0.15	0.27	0.27	0.14	0.13	0.27
Q_{pk}	0.49	0.43	0.39	0.40	0.45	0.38	0.40	0.45	0.38	0.44	0.45	0.31	0.25	0.40

Table 3. Root-mean-square (rms) errors for reconstruction results for standard reference points of the sinus rhythm (peaks of P, R, S, and T waves) in the presence of a 40-db noise and when using BEM. See Table 1 for explanations of acronyms describing regularization methods.

	ZOT	FOT	SOT	ZCG	FCG	SCG	ZLSQR	FLSQR	SLSQR	TSVD	ν	FTV	STV	LASSO
P	0.47	0.43	0.42	0.47	0.45	0.45	0.47	0.45	0.45	0.51	0.48	0.37	0.41	0.45
R	0.45	0.40	0.39	0.40	0.40	0.38	0.40	0.40	0.38	0.42	0.43	0.35	0.33	0.40
S	0.48	0.42	0.40	0.47	0.45	0.44	0.47	0.45	0.44	0.50	0.49	0.37	0.40	0.45
T	0.27	0.16	0.16	0.26	0.16	0.16	0.26	0.16	0.16	0.27	0.26	0.17	0.16	0.26

4. Discussion and conclusions

This study compared the performance of various regularization techniques using a unified computational framework derived from a realistic torso model with a canine heart. Our main finding is that non-quadratic methods (FTV and STV) have proven more robust to the complexity of the spatial patterns and noise in reconstructing the cylindrical-cage potentials. This conclusion is in agreement with the recent study of Gosh and Rudy [4], who noted that FTV method (also called L1 regularization) may better capture the spatial patterns of epicardial potentials than other techniques, which minimize the square of the norm.

Our future work includes developing experimental protocols that will identify the sites of early activation during pacing and in the circumstances of infarcted hearts.

References

[1] Oster HS, Taccardi B, Lux RL, Ershler PR, Rudy Y. Noninvasive electrocardiographic imaging: Reconstruction of epicardial potentials, electrograms, isochrones and localization of single and multiple electrocardiac events. Circulation 1997, **96:** 1012-1024.

[2] Brooks DH, Srinidhi KG, MacLeod RS, Kaeli DR. Multiply constrained cardiac electrical imaging methods. Subsurface Sensors and Applications, Proc. SPIE 3752, pp.62-71, 1999.

[3] Hren R. Value of epicardial potential maps in localizing pre-excitation sites for radiofrequency ablation. A simulation study. Phys. Med. Biol. 1998, **43**:1449-1468.

[4] Ghosh S, Rudy Y. Application of L1-norm regularization to epicardial potential solution of the inverse electrocardiography problem. Ann. Biomed. Eng. 2009, **37**: 902-912.

[5] Horacek BM, Clements JC. The inverse problem of electrocardiography: a solution in terms of single- and double-layer sources of the epicardial surface. Math Biosci 1997, **144**: 119-154.

[6] Tikhonov A, Arsenin V. Solution of Ill-Posed Problems. Washington, DC: Winston, 1977.

[7] Brooks DH, Ahmad GF, MacLeod RS. Inverse electrocardiography by simultaneous imposition of multiple constraints, IEEE Trans. Biomed. Eng. 1999, **46**: 3-18.

[8] Hanke M. Conjugate Gradient Type Methods for Ill-Posed Problems. Harlow: Longman Scientific & Technical, 1995.

[9] Paige CC, Saunders MA. LSQR: An algorithm for sparse linear equations and sparse least squares, ACM Transactions on Mathematical Software 1982, **8**: 43-71.

[10] Hansen PC. Rank-Deficient and Discrete Ill-Posed Problems. Philadelphia: SIAM, 1998.

[11] Schmidt M. Least Squares Optimization with L1-Norm Regularization, Project Report , University of British Columbia, 2005

Address for correspondence

Matija Milanič, PhD
Institute Josef Stefan
Jamova 39
1000 Ljubljana
Slovenia
E-mail address: matija.milanic@ijs.si